Forschungszentrum Karlsruhe

Technik und Umwelt

Wissenschaftliche Berichte

FZKA 6561

Continuum models for pebble beds in fusion blankets

L. Bühler

Institut für Kern- und Energietechnik
Programm Kernfusion

Forschungszentrum Karlsruhe GmbH, Karlsruhe
2002

Impressum der Print-Ausgabe:

Als Manuskript gedruckt

Forschungszentrum Karlsruhe GmbH
Postfach 3640, 76021 Karlsruhe

Mitglied der Hermann von Helmholtz-Gemeinschaft
Deutscher Forschungszentren (HGF)

ISSN 0947-8620

Continuum models for pebble beds in fusion blankets

Abstract

Continuum models for granular materials in fusion blankets are outlined. The work focuses on the capabilities of the ABAQUS finite element code which is used for the calculations. Special attention is paid on the modelling of the nonlinear elastic behavior of the pebble beds, granular particle flow caused by shear, volume compaction and hardening, and thermal creep. The derived material model gives results which are in reasonable accordance with known experimental data. The models are calibrated or verified for Li_4SiO_4. Nevertheless they are relatively general so that an application to other materials is straightforward.

Kontinuumsmodelle für Schüttbetten in Fusionsblankets

Zusammenfassung

Dieser Bericht beschreibt Kontinuumsmodelle zur Simulation des mechanischen Verhaltens granularer Medien in Fusionsblankets. Die Beschreibung orientiert sich an den Fähigkeiten des Finite Elemente Programms ABAQUS, das für die Berechnungen verwendet wird. Besondere Aufmerksamkeit gilt der Modellierung des nichtlinearen elastischen Verhaltens von Schüttbetten, granularem Fliessen von Partikeln, volumetrischer Kompaktierung und Hardening und thermischem Kriechen. Das entwickelte Material modell beschreibt das Verhalten in ausreichender Übereinstimmung mit experimentellen Daten. Die Stoffgesetze wurden für Li_4SiO_4 geeicht bzw. validiert. Die Modelle sind jedoch relativ allgemein, so dass eine Anwendung auch für andere Materialien nach einer entsprechenden Eichung möglich sein sollte.

Continuum models for pebble beds in fusion blankets

Contents

1 Introduction

For a reliable design of fusion blankets with breeding pebble beds it is important to have validated computational tools for predicting the thermomechanical conditions like stresses, strains, or heat transfer. An early blanket using pebble beds as breeding material had been proposed by Dalle Donne, Fischer, Norajitra, Reimann and Reiser (1995). Recently improved and advanced versions have been considered by Hermsmeyer, Gordeev, Kleefeldt, Schleisiek, Schmuck, Schnauder, Fischer, Malang, Fütterer and Ogorodnikowa (1999) and Boccaccini (2000), respectively. All these blankets have in common that the breeder region is split into a number of subregions, alternatingly filled with the breeding ceramic material e.g. lithiumorthosilicate, Li_4SiO_4, and the neutron multiplier beryllium, Be. Both materials are used in the form of small spheres as compact assemblies of granular material. The walls separating the breeder from Be have internal cooling channels through which the fusion heat is removed by high-pressure helium flow. The breeding product tritium required as "plasma fuel" in the fusion process is removed from the packed beds by a low-pressure helium purge flow.

The special design described above requires a high thermal contact between the granular particles themselves and between particles and the cooling walls in order to keep the temperature induced in the bed by internal heat release within acceptable limits. The thermal expansion of the granular filling and the irradiation swelling of the particles may be favorable for heat transfer reasons. The stresses within the granular material lead to a local increase in the contact areas between particles and thus to an increase of the heat transfer properties.

On the other hand, the stresses created in the particles by their volumetric expansion may become so large, that some fraction of the particles will be destroyed or the wall material may fail during operation of the blanket. However, Reimann and Wörner (2000) showed recently that if the material becomes ductile at the maximum operating temperatures near 900 °C the particles will exert a plastic deformation due to thermally activated creep. The particles may remain entirely intact but exhibit permanent plastic deformations mainly near their contact areas. These plastic deformations can not be recovered during thermal cycles when the beds reach lower temperatures such as 350 °C.

It is assumed in this report that the beds retain their cohesionless granular behavior. There is a possibility that the granular bed may reduce high local stresses by macroscopic movements of intact particles. Such consolidation of the beds is possible if the initial packing density was not the highest possible one. Internal forces between particles may contribute to consolidation processes but also movements along larger distances seem possible supposed that the beds find enough space for an expansion. Such effects are known especially from soil mechanics (see e.g. Nedderman (1992)) and various models exist do describe such phenomena as shown in figure 3. The figure displays typical results shown by Reimann, Müller, Arbogast and Thomauske (1998) for cyclic uniaxial compression. During an initial increase of the load the sample undergoes irreversible deformation due to a rearrangement of particles and reversible deformation due to elasticity of the bed. The latter fraction becomes visible if the load is decreased and increased again. Cycling loads to a continuous compaction which indicated that the bed had not the most dense initial packing. After a large number of cycles the results converge toward a closed curve which is dominated by nonlinear elasticity. The small

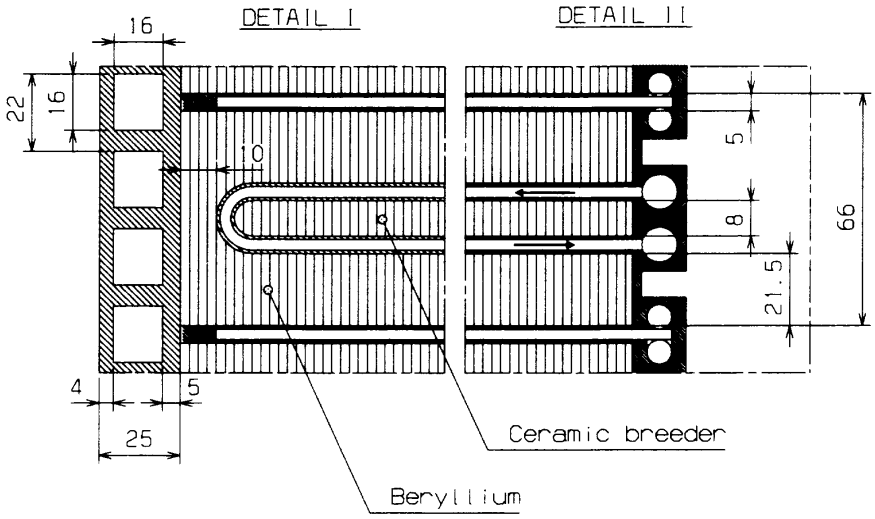

Figure 1: Part of an improved Helium Cooled Pebble bed Blanket (Hermsmeyer et al. (1999))

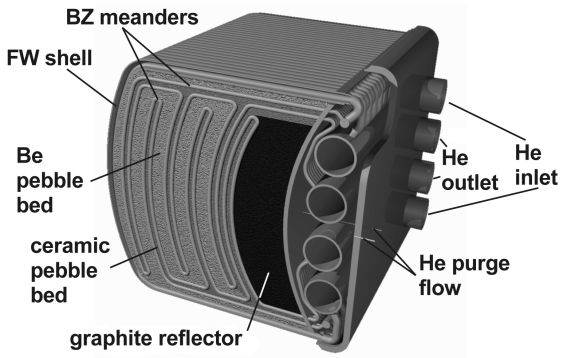

Figure 2: View of an Advanced Helium Cooled Pebble bed Blanket (Boccaccini (2000))

hysteresis may be caused by minor friction effects.

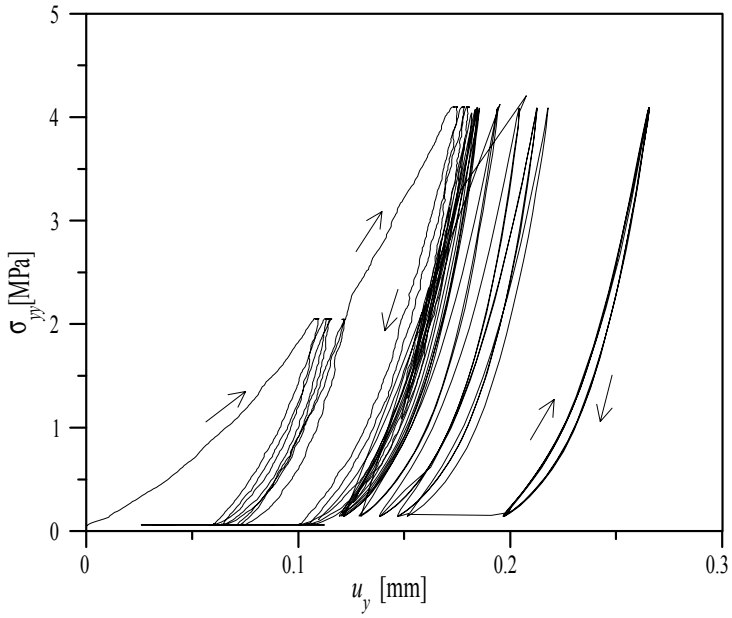

Figure 3: Cyclic oedometric compression of Li_4SiO_4 at 400 °C as shown by Reimann et al. (1998).

A theoretical description is obtained by using constitutive equations to describe the granular behavior on a macroscopic scale, i.e. the granular assembly whose characteristic dimensions are large compared with the particle size is treated as a continuum. We outline in the following models which account for nonlinear elasticity, irreversible volume compaction during compression, shear failure and granular flow (movement) of particles and thermally activated creep. These effects should dominate the thermomechanical behavior of confined dense pebble beds.

2 Characterization of granular materials

Granular materials are characterized both by the particle density ρ_s and most importantly by the bulk density ρ_b. For the same value of ρ_s different values for the bulk density ρ_b are possible, "depending on the manner in which the vessel is filled. The bulk density is found to increase with the application of elevated stresses or when the sample is vibrated." (Nedderman (1992)) The bulk density is related to the void fraction ε (volume fraction occupied by the interstitial medium with density ρ_g) as

$$\rho_b = (1-\varepsilon)\,\rho_s + \varepsilon\rho_g. \tag{1}$$

For the applications considered the interstitial medium is a gas with $\rho_g \ll \rho_s$ so that the relation above simplifies to

$$\rho_b = (1-\varepsilon)\,\rho_s. \tag{2}$$

The specific volume v is the ratio of volume of the sample to the volume of the solid and is related to the so called voids ratio

$$e = \frac{\varepsilon}{1-\varepsilon} \tag{3}$$

as

$$v = 1 + e. \tag{4}$$

There is a number of other physical parameters that may characterize an assembly of granular particles (like particle size, particle shape, particle porosity, thermal and electrical properties, ... see e.g. Nedderman (1992)). The breeder particles Li_4SiO_4 foreseen in fusion blankets are much smaller than the dimensions of the containers. Therefore one can assume that the shape and size are of minor importance so that the relations given just above may be sufficient for the further description of the mechanical behavior.

The granular material is constrained by walls and therefore differences in thermal expansion between the wall material and the granular bed will cause thermal stresses. On the other hand one can imagine that the beds have initial compression created by the filling procedure. Some initial stresses are desirable in order to avoid gap formation near the walls or to ensure higher thermal conductance compared with unconstrained beds. For many purposes it is convenient to decompose the stress tensor $\boldsymbol{\sigma}$ into a deviatoric part $\mathbf{S}$ and into a spherical part $-p\mathbf{I}$ as

$$\boldsymbol{\sigma} = \mathbf{S} - p\mathbf{I}, \tag{5}$$

where $p = -\frac{1}{3}\mathrm{trace}(\boldsymbol{\sigma})$ is called the pressure (see e.g. Durelli, Phillips and Tsao (1958)). This decomposition allows an evaluation of the Mises equivalent stress as

$$q = \sqrt{\frac{3}{2}\mathbf{S} : \mathbf{S}} \tag{6}$$

and the third stress invariant becomes

$$r = \left(\frac{9}{2}\mathbf{S} : \mathbf{S} \cdot \mathbf{S}\right)^{1/3}. \tag{7}$$

2.1 Elasticity

A material is called a *Cauchy elastic solid* if there exits a unique relation between the stress tensor $\boldsymbol{\sigma}$ and the deformation

$$\boldsymbol{\sigma} = \mathbf{f}(\mathbf{F}), \tag{8}$$

where $\mathbf{F}$ is the displacement gradient matrix (Hunter (1983)). In the isotropic case the most simple form of equation (8) is the linear version, known as Hook's law

$$\boldsymbol{\sigma} = \lambda(\nabla \cdot \mathbf{u})\mathbf{I} + 2\mu\mathbf{e}. \tag{9}$$

In this notation the pressure reads as

$$p = -\left(\lambda + \frac{2}{3}\mu\right)\mathrm{trace}(\mathbf{e}). \tag{10}$$

The vector $\mathbf{u}$ stands for the displacement and $\mathbf{e}$ is the matrix of the strain components which reads for the *small displacement gradient approximation* in spatial coordinates x_i:

$$e_{ij} = \frac{1}{2}\left(\frac{\partial u_i}{\partial x_j} + \frac{\partial u_j}{\partial x_i}\right). \tag{11}$$

The change in volume is $\nabla\cdot\mathbf{u}$ =trace $(\mathbf{e})$ and the parameters λ, μ are the Lamé constants. The parameter μ is also known as the shear modulus. According to equation (10) the pressure is related to the first strain invariant as

$$p = -K\,\mathrm{trace}(\mathbf{e}) = -K\Delta V/V = K\varepsilon_{vol} \tag{12}$$

where K is the ratio of hydrostatic pressure to the applied volume shrink or volumetric strain, $\varepsilon_{vol} = -\Delta V/V$. This property is known as the bulk modulus and can be expressed with the Lamé constants as

$$K = \lambda + \frac{2}{3}\mu. \tag{13}$$

It is possible to invert equation (9) and find

$$\mathbf{e} = \frac{1}{2\mu}\left(\boldsymbol{\sigma} + \frac{3\lambda}{3\lambda + 2\mu}p\mathbf{I}\right) \tag{14}$$

or in terms of the *Poisson ratio* $\nu = \frac{\lambda}{2(\lambda+\mu)}$

$$\mathbf{e} = \frac{1}{2\mu}\left(\boldsymbol{\sigma} + \frac{3\nu}{1+\nu}p\mathbf{I}\right). \tag{15}$$

The equations displayed above describe the elastic behavior of a solid body. The elasticity of a sample of granular particles in form of cylinders (2D models) or spheres (3D applications), however, deviates from that of a solid sample of the same material. If the solid sample has a linear relation between stress $\boldsymbol{\sigma}$ and strain $\mathbf{e}$ according to equation (9), this is not necessarily the case for granular assemblies as can be shown in experiments.

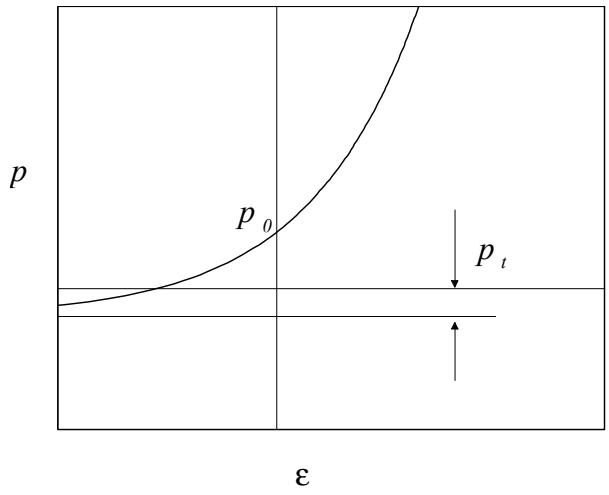

Figure 4: Porous elastic volumetric behavior

2.2 Porous elasticity

The behavior of a volume of granular particles during compression is quite different from that of a solid sample of same size and material. While for a solid sample the elastic parameters are constant over a wide range of the applied stresses a granular assembly of the same material shows a pronounced load dependence of these quantities.

It has been shown that the elastic behavior of dense packings of Li_4SiO_4 can be explained by Hertz contact between particles (Walton (1987), Endres (1990)). Contacts exist between a number of particles and additional contacts are generated between points which were initially at some distance. Such a simple model is able to reproduce experimental observation with sufficient accuracy and may help to get some insight into the physics involved. Nevertheless, it is not suitable for practical use. In the following a nonlinear elastic law is outlined that is more or less empirical but is available in standard finite element codes. We use experimental results to calibrate the constitutive models in the ABAQUS finite element code (*ABAQUS / Standard* (1996)) for applications to fusion blankets. This code allows a flexible modelling of nonlinear elastic material properties by the use of the ∗*porous elasticity* option. Using the definitions introduced above the elastic part of the change in volume is accurately modeled by

$$\frac{\Delta V}{V} = -\varepsilon_{vol} = \frac{\kappa}{1+e_0} \ln\left(\frac{p_0+p_t}{p+p_t}\right). \tag{16}$$

Here, e_0 is the initial voids ratio and κ is the so-called *logarithmic bulk modulus*. The quantity p_0 characterizes the initial stress state and p_t the *elastic tensile strength in the sense that* $\Delta V/V \to \infty$ as $p \to -p_t$. For a granular assembly p_t looses the physical meaning since the pressure is always positive, $p > 0$, but it serves as a parameter to fit the experimental data.

The *porous elasticity* option requires additionally to the input data described above the value of a Poisson ratio ν^* for the granular bed. Since no information exists on this property it is assumed that $\nu^* = 0.05$, a value that is between the theoretical limit for

perfectly smooth particles ($\nu^* = \frac{1}{4}$) and perfectly rough ones ($\nu^* = \frac{\nu}{2(5-3\nu)}$) in random packings of spheres (Walton (1987)).

2.3 Granular flow

The elastic parts of the experimental curves can be reproduced well with the simple porous elastic option. To account for permanent plastic deformations (consolidation) during the initial compression the material model must be extended. The deficiency to deal with plastic deformations while using elastic models can be removed by using the Drucker-Prager cap model to describe more realistically the material behavior. What is described below is related to the capabilities of the ABAQUS FE code and can be found in the Theory- and User's Manual *ABAQUS / Standard* (1996).

The material is assumed to behave as a nonlinear (porous) elastic body as long as the stress state lies within a volume in stress space, the surface of which is called the yield surface. A typical yield surface is shown in figure 5 as a curve in a $p-t$ plane. The variable $p = -\text{trace}(\boldsymbol{\sigma})$ denotes, as introduced above, the pressure stress and t stands for a measure of tangential (deviatoric) stresses. The variable t can be related to the Mises equivalent stress $q = \sqrt{\frac{3}{2}\mathbf{S} : \mathbf{S}}$ and to the third stress invariant $r = \left(\frac{9}{2}\mathbf{S} : \mathbf{S} \cdot \mathbf{S}\right)^{1/3}$ as

$$t = \frac{1}{2}q\left[1 + \frac{1}{K} - \left(1 - \frac{1}{K}\right)\left(\frac{r}{q}\right)^3\right], \tag{17}$$

where $0.778 \leq K \leq 1$ is a material parameter that controls the dependence of the yield surface on the value of the intermediate principle stress as shown in figure 6. The value of K used in the following is chosen to $K = 1$, as advised by the ABAQUS manual if it is desired to be used in conjunction with creep (to be used in a further step). Then the equation displayed above reduces to

$$t = q. \tag{18}$$

Returning to Fig. 5 one can recognize that the yield surface is built up by a linear part, the Drucker-Prager *shear failure surface*,

$$F_s = t - p\tan\beta - d = 0, \tag{19}$$

and the so-called *cap,*

$$F_c = \sqrt{(p - p_a)^2 + \left(\frac{Rt}{1 + \alpha - \alpha/\cos\beta}\right)^2} - R\,(d + p_a\tan\beta) = 0. \tag{20}$$

The parameters involved in this definition can be seen from Fig. 5. For a smooth connection a transition surface, F_t is introduced.

The material is about yielding by shear if the stress state lies on F_s. Shear occurs when the tangential (deviatoric) stresses exceed values that depend linearly on the normal stress. Such a behavior is closely related to Coulomb friction. The parameter β is known as the material's friction angle. For cohesionless granular materials the parameter d vanishes, $d = 0$. The Code input, however, requires $d > 0$. For this reason, the input of d is chosen positive but as small as possible, $d = 1 \cdot 10^{-6}$. In the equations

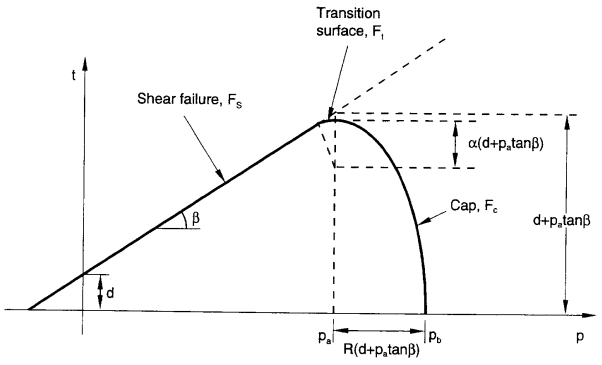

Figure 5: Yield surface in the $p-t$ plane *ABAQUS / Standard* (1996)

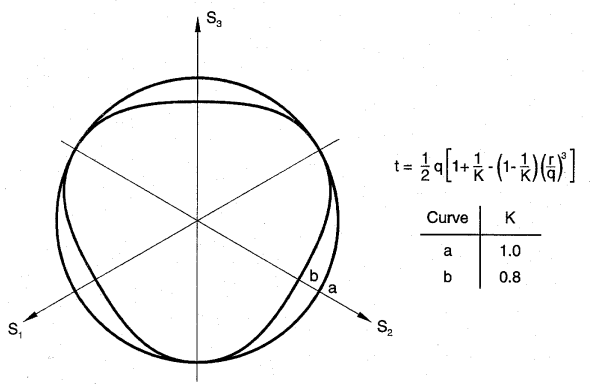

Figure 6: Typical yield/flow surfaces in the deviatoric plane *ABAQUS / Standard* (1996).

displayed above α is a small parameter that helps to connect smoothly the cap and the shear failure line. Its value is set to $\alpha = 0$ as advised by the ABAQUS manual if it is desired to be used in conjunction with creep (to be used in a further step).

The material is about yielding by compression (consolidation) if the stress state lies on F_c.

Plastic shear and compression are described by the flow potentials,

$$G_s = \sqrt{(p_a - p)^2 \tan^2 \beta + \left(\frac{t}{1 + \alpha - \alpha/\cos\beta}\right)^2} \tag{21}$$

and

$$G_c = \sqrt{(p - p_a)^2 + \left(\frac{Rt}{1 + \alpha - \alpha/\cos\beta}\right)^2}, \tag{22}$$

respectively. Plastic flow with strain rates

$$\dot{\mathbf{e}} \sim \frac{\partial G}{\partial \boldsymbol{\sigma}} \tag{23}$$

will last as long as the stress state lies beyond the yield limit. The flow rule is non-associated since the flow potential and the yield function are different. The flow will stop when either stresses are released to tolerable values by the flow, or for the case, when the yield surface itself is modified by the flow such that a stable state is reached again. A modification of the yield surface is possible by cap hardening by which the cap position p_b and consequently the value p_a is related to the current state of deformation.

2.4 Hardening

During compression the granular material undergoes hardening for various reasons. Without modelling the details one can describe the macroscopic observations by the definition of the cap hardening parameters $p_b\,(\varepsilon_{vol,pl})$ which defines the cap position and fixes the parameter p_a in the yield function and in the flow potential. The representation in form of a power law as

$$p_b = \hat{p}_b \left(\frac{\varepsilon_{vol,pl}}{\hat{\varepsilon}_{vol,pl}}\right)^a \tag{24}$$

has enough degrees of freedom for fitting the experimental observations with sufficient accuracy. Here $\hat{p}_b$ and $\hat{\varepsilon}_{vol,pl}$ are typical magnitudes and n is an exponent. For vibrated Li_4SiO_4 pebble beds at room temperature these values are close to $\hat{p}_b \approx 3.3$ MPa, $\hat{\varepsilon}_{vol,pl} \approx 3.33 \cdot 10^{-3}$ and $a \approx 1.66$.

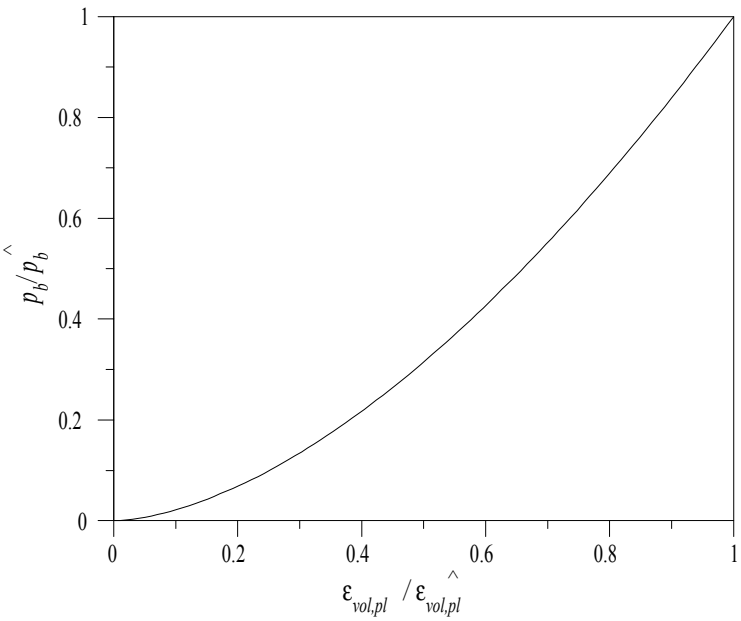

Figure 7: Cap hardening for Li_4SiO_4 with $\hat{p}_b = 3.3$ MPa and $\varepsilon_{vol,pl} = 0.0033$.

3 Calibration and applications

We apply the granular models to experiments performed by Reimann and co-workers for calibration of the material input data and for validation of the used models. One of these experiments has been described already e.g. by Bühler, Reimann, Arbogast and Thomauske (2000) but the main features are briefly outlined in the following. The spherical breeder pebbles with diameters between 0.25 mm and 0.65 mm are filled into a cavity as shown in Fig. 8 and experiments are performed at room temperature. The investigated geometry consists of a flat granular bed closed by a rigid plate at the top which is loaded at its center by an external force F_y to simulate the thermal stresses in the blanket. The position of the plate center is at $y = L_y$ and the plate may rotate around the z-axis by a small angle α. The cavity is built by rigid fixed walls at $x = 0$ and $y = 0$. At $x = L_x$ the bed is confined by a piston that has translational degree of freedom along x to allow for a balance of the reaction force created by the horizontal stress σ_{xx} in the bed with the externally applied force F_x. If the bed reaction force is smaller than F_x the piston is fixed mechanically at its initial position L_{x0}. The vertical and horizontal forces are divided by the areas on which they act and represented in the following as $\bar{\sigma}_{yy}$ and $\bar{\sigma}_{xx}$, respectively. The other rigid walls that confine the cavity in z-direction are fixed at a distance L_{z0}. The vertical dimension of the experiment is close to the blanket scale for the breeder gap with a height $H_0 = 0.011\,\mathrm{m}$. The lateral extensions along the coordinates x and z are chosen much larger than the height, with $L_{x0} = L_{z0} = 0.1\,\mathrm{m}$. The contact between wall and granular material is described using a measured coulomb friction coefficient $\mu_w = 0.25$. This is important especially for modelling since the bed may be in sliding or sticking contact, depending on the ratio of normal and tangential stress.

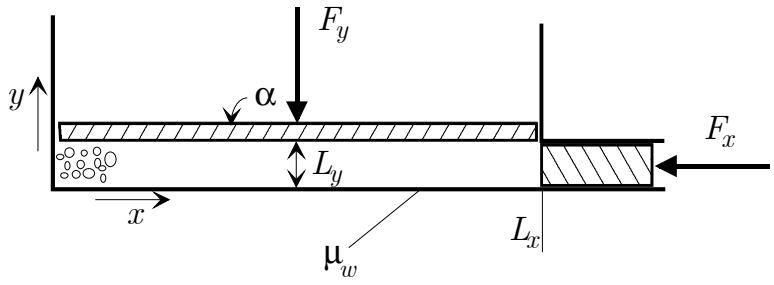

Figure 8: Sketch of the experimental geommetry

In order to describe theoretically the pebble bed behavior, results from uniaxial compression tests are needed. These tests are performed in the same test section, keeping the horizontal piston fixed at L_{x0} and recording the vertical compaction, the change in L_y, as a function of $\bar{\sigma}_{yy}$. The simultaneous measurement of $\bar{\sigma}_{xx}$ is a valuable quantity. Uniaxial compression data are available in addition from other experiments performed in cylindrical cavities. As long as these experiments are performed at room temperature they show essentially the same behavior (compare e.g. with Reimann and Müller (1998)).

For investigating the biaxial particle movements the load $\bar{\sigma}_{yy}$ is increased monotonically while $\bar{\sigma}_{xx}$ can not exceed a certain value. The volumetric compaction of the bed

is measured by recording at the plate the vertical position $L_y = H_0 + u_y$ and the horizontal position of the piston $L_x = L_{x0} + u_x$, where u_y and u_x are vertical and horizontal displacements, respectively. In addition the experiment allows for recording of α and for measuring whether the system is really two dimensional by having some sensors out of the symmetry plane $z = 0$. The two-dimensional behavior is essential for the application of plane strain conditions during the analysis.

3.1 Uniaxial compression

A calibration for the elasticity model and for the cap hardening input is done by a comparison of computed data with the uniaxial compression experiments. The adjusted values are used later for the biaxial flow applications. Figure 9 shows a comparison of measured data and calculated results both for loosely filled beds and for vibrated beds. It is possible to reproduce the loading curve with sufficient agreement. The vertical load is increased up to the maximum value in about 15 min and kept constant for 1h. The ongoing compression during the period of constant load indicates that quasi steady state conditions were not completely reached. The assembly needs some time in order to find the final state. However, the deformations during this period are small compared to the deformation due to compression during the loading part. Later, the load is reduced. The bed expands again, but does not reach its initial extension.

Figure 9 demonstrates moreover the dominating influence of the initial treatment of the bed. If the bed is loosely filled one finds larger deformations during compression than for the case when the bed is initially vibrated even if the void fractions of both experiments are similar. The differences caused by different filling methods are even more pronounced if one considers the stresses caused by the same displacements u_y. The results for $\bar{\sigma}_{yy}$ then can deviate at least by one order of magnitude between loosely filled and initially vibrated beds. It is important to notice that the volumetric expansion during blanket operations is most likely related to the latter case. Therefore it is recommended that experiments should be performed carefully, using the same densification method (e.g. vibrations) as in the blanket. In addition, experiments should be repeated to ensure reproducible results.

For obtaining the numerical data displayed in Fig. 9 two different material input data sets were created, one for the vibrated beds and one for the loosely filled beds. They differ essentially in the cap hardening data. While it is possible to fit the experimental data for vibrated beds well with $\hat{\varepsilon}_{vol,pl} \approx 3.33 \cdot 10^{-3}$ a value of $\hat{\varepsilon}_{vol,pl} \approx 1.27 \cdot 10^{-2}$ is required for the loosely filled beds for the reference pressure $\hat{p}_b \approx 3.3$ MPa. The exponent in the power law (24) for the cap position is $a \approx 1.66$ and does not depend on the initial treatment. The cap hardening curves used are shown in Fig. 10.

The horizontal force necessary to keep the piston at its initial position has been recorded and results are shown in Fig. 11. During compression the lateral load $\bar{\sigma}_{xx}$ is roughly related linearly with the vertical one $\bar{\sigma}_{yy}$ reflecting the constant angle of internal friction. The value $\bar{\sigma}_{xx}$ stays at large values when the vertical load is released and returns to zero for small $\bar{\sigma}_{yy}$. Note, during this experiment the bed height was about twice as high as the vertical extension of the piston.

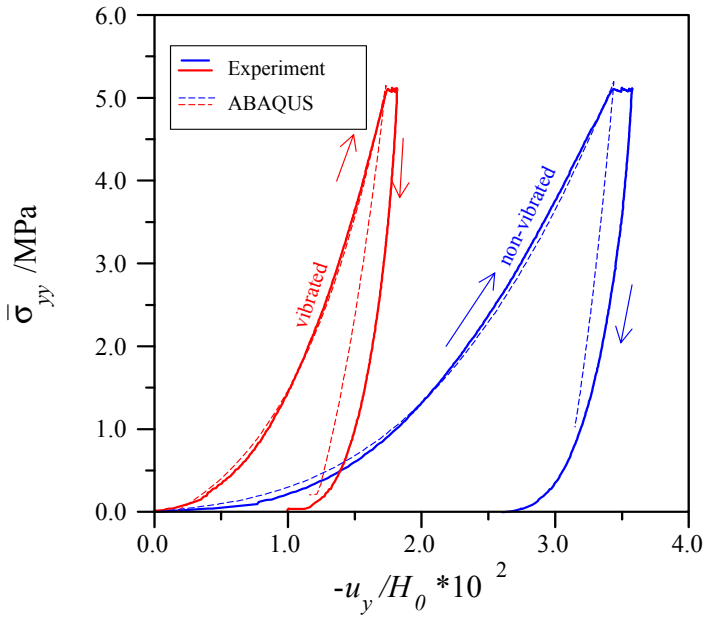

Figure 9: Uniaxial compression; $\bar{\sigma}_{yy}$ versus u_y for a loosely filled and initially vibrated breeder bed. Comparison of experimental and numerical data.

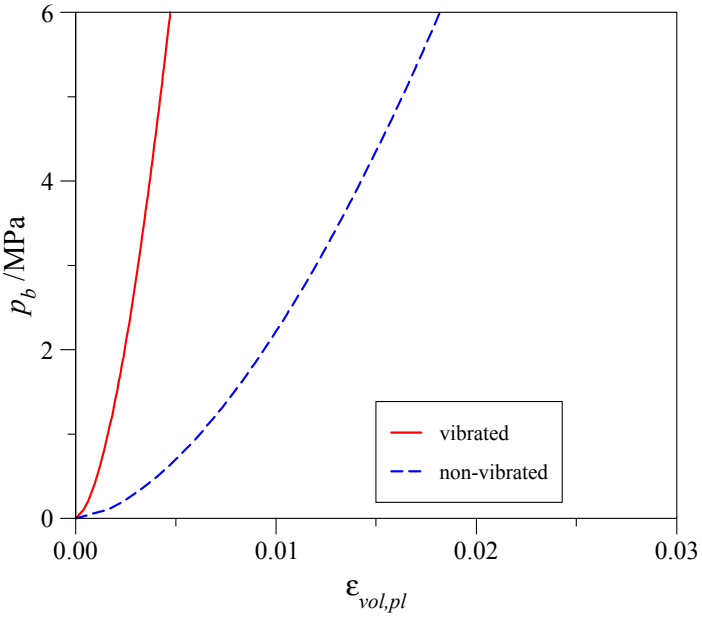

Figure 10: Cap hardening data used in ABAQUS for calculations of uniaxial compression experiments.

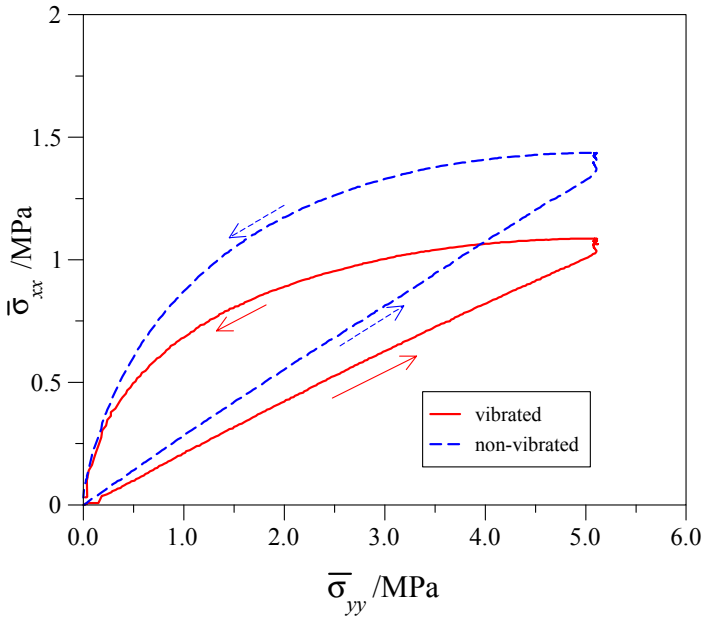

Figure 11: Uniaxial compression; $\bar{\sigma}_{yy}$ versus $\bar{\sigma}_{xx}$ for loosely filled and initially vibrated Li_4SiO_4 beds.

3.2 Biaxial granular flow

In the following section results are shown for the case when during vertical compression the horizontal piston can move. The biaxial particle flow experiments were performed in such a way that the vertical load was increased up to the maximum value of about $\bar{\sigma}_{yy,max} = 5\,\mathrm{MPa}$ in a given time period (2 h for the experiments with $\bar{\sigma}_{xx} = 0.058,\ 0.12,$ and 0.4 MPa, and 16 h for $\bar{\sigma}_{xx} = 0.075\,\mathrm{MPa}$), then the load was kept constant for 2 h and finally, the force was reduced to zero during 15 min. When the vertical force is increased above a certain value, depending on $\bar{\sigma}_{xx}$ the horizontal piston starts to move. It moves more or less linearly with increasing vertical force over a wide range (see Fig. 12).

The important result is that the values u_x are very small: for $\bar{\sigma}_{xx} = 0.4\,\mathrm{MPa}$ the maximum horizontal displacement of particles becomes roughly $u_x/H_0 = 10^{-2}$ (corresponding to 0.1 mm) at the highest vertical load. Even the maximum displacement of about $u_x/H_0 = 4 \cdot 10^{-2}$ (0.4 mm) for $\bar{\sigma}_{xx} = 0.075\,\mathrm{MPa}$ is not very large considering the very small horizontal load compared with the maximum vertical one. The experimental observations are compared with ABAQUS calculations using an internal friction angle of $\beta = 44°$. The agreement is satisfactory and deviations are within the range of experimental accuracy.

Not shown in the figures are the displacements u_y as a function of $\bar{\sigma}_{yy}$. The fact that the horizontal dimension extends monotonically leads to the result that larger vertical displacements are possible now for the same vertical loads compared with the uniaxial compression tests.

In addition to the vertical displacement the inclination angle α of the top plate is recorded and plotted versus the displacement u_x of the horizontal piston. The results are shown in Fig. 13. The granular material is displaced in the x-direction near $x = L_x$ and

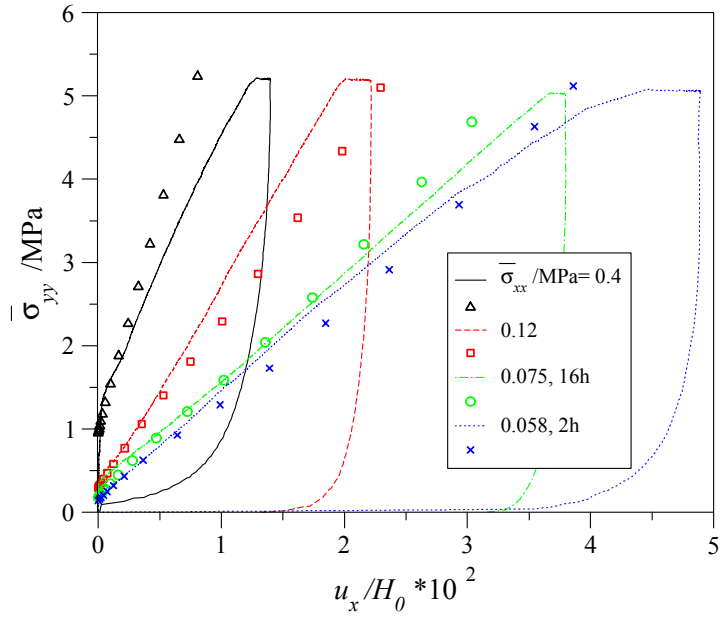

Figure 12: Vertical load versus horizontal displacement of the piston u_x for $\bar{\sigma}_{xx} = 0.058 \div 0.4\,\mathrm{MPa}$ for vibrated beds. Symbols denote ABAQUS calculations.

the stress (or the pressure) is locally released. This gives an unbalanced stress acting on the plate with the result that the plate turns by an angle α. With increasing inclination the granular bed is less compressed near $x = 0$ so that in a final balanced state one finds high pressure near the center $x = L_x/2$ and reduced loads almost symmetrically distributed around the center, although the bed can expand laterally only at the right side. One finds from calculations almost a linear relation between α and u_x with only marginal dependence on the lateral confinement. During experiments this tendency is confirmed especially for low lateral constraints and for the case when the load is applied over a long period of 16 h. Experiments which are performed on smaller time scales deviate from the predictions with increasing lateral force. The reason is unclear for the moment but could be attributed to friction effects or transient behavior in the experiment especially at high and fast loads. This point needs further investigations. The experimental curve bends at the position where the vertical force is released. Then the piston is pushed back and the plate is tilted towards its initial orientation.

Some experiments have been performed with loosely filled beds. Already the uniaxial tests showed that the physical behavior is quite different. Biaxial experiments plotted in Fig. 14 show larger horizontal displacements for same vertical loads compared with the vibrated case. This indicates that the internal friction angle β is influenced by the filling method. This is also confirmed by Fig. 11, where different slopes have been measured for both types of filling. The result here is that about three times larger displacements u_x are to be expected in loosely filled beds compared with the initially vibrated beds. A friction angle $\beta \approx 41^\circ$ was found to describe the situation with reasonable accordance with the experimental data.

The inclination is reproduced qualitatively by the calculations. It is found, however,

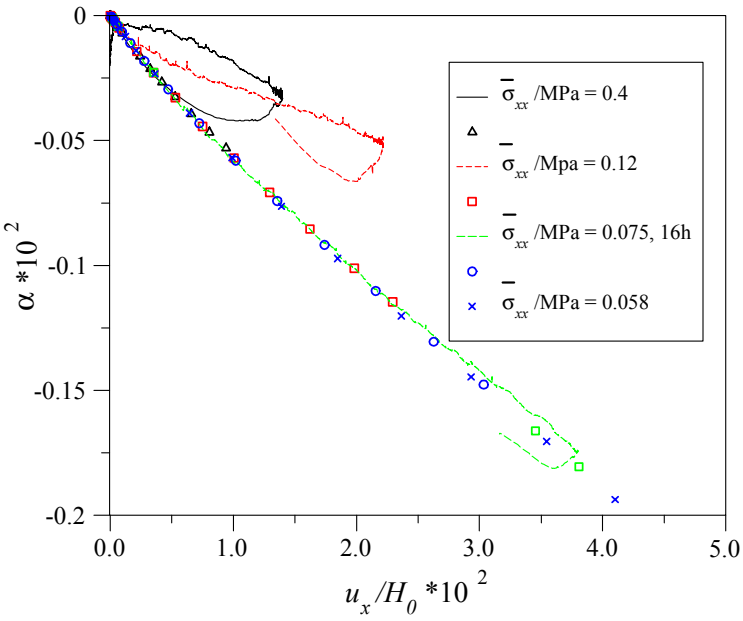

Figure 13: Change of inclination angle α with horizontal displacement u_x for $\bar{\sigma}_{xx} = 0.058 \div 0.4\,\mathrm{MPa}$ for vibrated beds. Symbols denote ABAQUS calculations.

that the magnitude is larger than observed in the experiment. One can speculate that if during the experiment the load would have been applied more slowly the agreement would have been better as it was the case for vibrated beds.

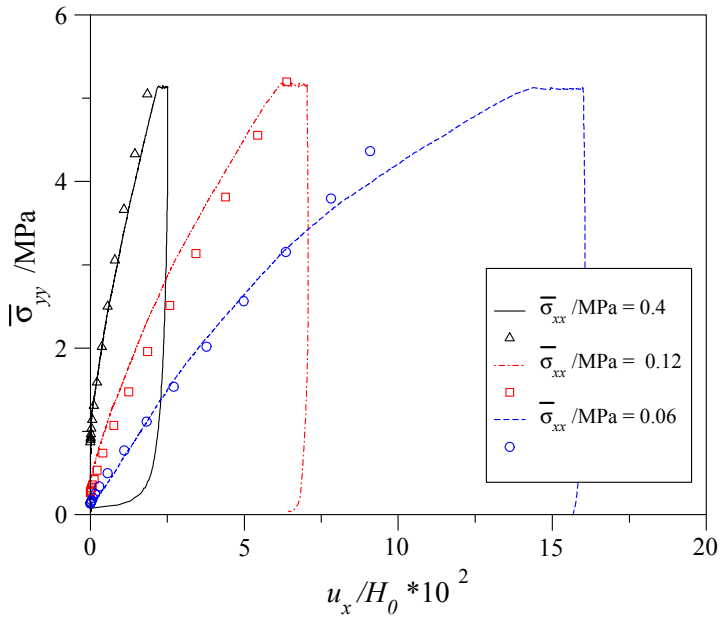

Figure 14: Vertical load versus horizontal displacement of the piston u_x for $\bar{\sigma}_{xx} = 0.06$, 0.12, 0.4 MPa for loosely filled beds. Symbols denote ABAQUS calculations.

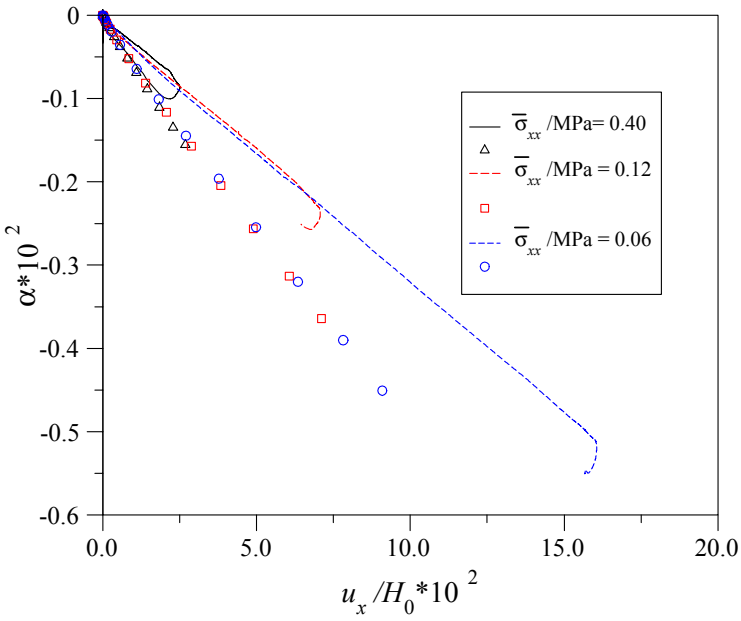

Figure 15: Change of inclination angle α with horizontal displacement u_x for $\bar{\sigma}_{xx} = 0.06$, 0.12, 0.4 MPa for loosely filled beds. Symbols denote ABAQUS calculations.

4 Thermal creep

Recent experiments showed that thermal creep of granular breeder materials becomes important at higher temperatures. If for example a bed of Li_4SiO_4 at 800 °C is compressed by a uniform vertical load of $\bar{\sigma}_{yy} = 4.2$ MPa the thermal creep strain exceeds already after one day the plastic and elastic strains occurring during the loading period so that thermal creep is essentially important for a realistic description of the long-term behavior of a fusion blanket with pebble beds.

Munz and Fett (1999) describe the creep behavior of solid samples of ceramic materials. They distinguish between a primary creep phase, a secondary creep phase and a tertiary creep phase. Since all experiments done so far with granular beds did not show the tertiary phase for the investigated time periods we do not address this phase here. The secondary creep phase is the one which is active over most of the time during experiments. Moreover, many materials do not exhibit a primary phase. Therefore we do not distinguish between primary and secondary creep in this report and when we talk about creep we suppose that the creep law is of the type

$$\dot{\varepsilon} = A\,(T)\,p^n t^m, \tag{25}$$

with a magnitude A depending on temperature T. In a granular bed creep will not occur with the same magnitude in the whole material. Especially at the surfaces where granular particles are in contact with each other we have the highest stresses so that the magnitude of the creep stain rate $\dot{\varepsilon}$ is larger than at other places in the particle where the stresses are much lower. During creep the contact areas increase. This reduces the local stresses for the same externally applied load so that $\dot{\varepsilon}$ is decreased. In addition initial gaps may close during creep compaction. This fact creates new contacts which transmit a fraction of the load and decreases the average stress per contact surface, resulting in lower creep strain rate $\dot{\varepsilon}$ with progressing time.

Let us support the creep law shown above with some heuristic arguments. Suppose a granular particle is in contact with its neighboring particles at the contact areas at which the force $\mathbf{F}$ is transmitted. We suppose further that the particles had initially locally spherical shapes before the contact areas have been deformed by the applied load. The situation is depicted in Fig. 16. In the following we denote the average compressive stress as $p \sim F/d^2$. During creep the radius of the contact area and the contact surface increase as $\varepsilon^{1/2}d$ and εd^2, respectively, where ε is proportional to the volumetric strain of the granular bed. Munz and Fett (1999) report that creep of a solid sample in the second phase often follows a law with constant strain rate as

$$\dot{\varepsilon} \sim \sigma^{\alpha}. \tag{26}$$

Such a relation may hold in our case near the contact region where the stress is related to the compressive granular load as

$$\sigma \sim \frac{F}{\varepsilon d^2} \sim \frac{1}{\varepsilon} p. \tag{27}$$

This yields with (26)

$$\dot{\varepsilon} \sim \left(\frac{1}{\varepsilon} p\right)^{\alpha} \tag{28}$$

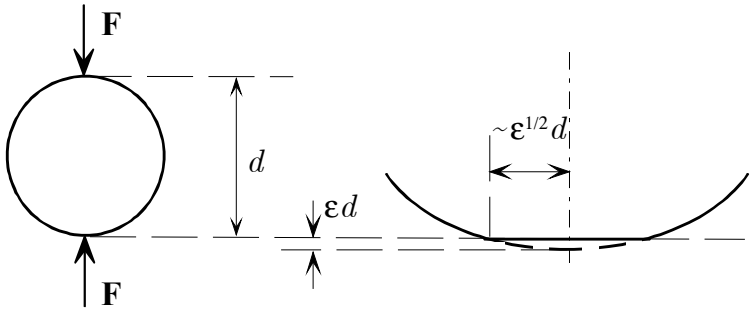

Figure 16: Sketch of a particle in creeping contact

and after integration

$$\varepsilon \sim p^{\frac{\alpha}{\alpha+1}} t^{\frac{1}{\alpha+1}} \quad \text{or} \quad \dot{\varepsilon} \sim p^{\frac{\alpha}{\alpha+1}} t^{\frac{-\alpha}{\alpha+1}} = p^n t^m. \tag{29}$$

This equation shows that even if a solid material has a constant creep velocity a granular bed with particles of the same material may have different behavior. The exponent m may be extracted form granular experiments to be close to $m \approx -0.8$. This means that the exponent α would have values about $\alpha \approx 4$, which is in the range as reported by Munz and Fett (1999) for ceramic materials under compression where e.g. $\alpha = 3.65$ for silicone carbide. The assumptions introduced so far oversimplify the real situation. This is manifested by an inaccurate prediction of the pressure dependence in (29) where the model would predict $n = -m$ which overestimates the measured pressure exponent $m_{measured} = 0.65$ (Reimann and Wörner (2000)). The deficiency of the model may be caused by the fact that the stress at the contact surface is not uniform and because the contact areas are estimated from simple geometric considerations without reference to precise deformations. We therefore chose the more general creep law (25) and show later that the degrees of freedom are sufficient to reproduce well the data obtained in creep experiments.

Creep for Drucker-Prager-Cap materials may consist of two contributions. One is the so-called cohesion creep while the other is the cap-creep causing consolidation of the sample. We assume that the granular material is cohesionless so that the relevant creep mechanism is consolidation. Plastic creep flow is determined by the strain rate tensor

$$\dot{\mathbf{e}} \sim \frac{\partial G_c}{\partial \boldsymbol{\sigma}}, \tag{30}$$

with the consolidation creep potential as foreseen in the ABAQUS cap creep option

$$G_c = \sqrt{(p - p_a)^2 + (Rq)^2}. \tag{31}$$

This standard cap creep potential is shown in Fig. 17 as the dashed sector of the cap. The magnitude of the strain rate is controlled by a constitutive equation defining the volumetric consolidation creep strain rate. For a strain hardening mechanism we have

$$\dot{\varepsilon}_c = \left(A\, \bar{p}_c^{\,n} \left[(m+1)\, \varepsilon_c\right]^m\right)^{\frac{1}{m+1}}. \tag{32}$$

For the creep pressure ABAQUS uses $\bar{p}_c = p - p_a$. The evaluation of (30) yields with $\partial q/\partial \boldsymbol{\sigma} = \mathbf{n}$ and $\partial p/\partial \boldsymbol{\sigma} = -\frac{1}{3}\mathbf{I}$

$$\dot{\mathbf{e}} = \dot{\varepsilon}_c \frac{1}{G_c}\left(R^2 q\,\mathbf{n} - \frac{1}{3}\bar{p}_c\,\mathbf{I}\right). \tag{33}$$

As we saw before in Fig. 5, the quantity p_a is closely related to the cap position p_b. During creep the cap position is shifted to higher values and as a consequence p_a as well. If the external load is kept constant the quantity $(p - p_a)$ decreases continuously during creep and vanishes finally. In case of isotropic compression we would loose the driving mechanism for creep and the material would "freeze". During experiments, however, creep magnitudes are observed which are much higher than those attainable with the above model. Therefore, the model may serve for a description only during some short initial state.

For modelling of short and long-term behavior another model is proposed and outlined in the following. The experiments showed that for a realistic description of creep the creep pressure foreseen in ABAQUS, $\bar{p}_c = p - p_a$ is irrelevant since creep does not stop when $p = p_a$. Therefore we chose the pressure stress as the effective creep pressure for our modelling as

$$\bar{p}_c = p. \tag{34}$$

This quantity is independent from the cap position and does not cause "freezing" of the creep process in accordance with experimental observations. For a definition of the creep strain rate tensor we define a new creep potential as

$$G_c = \sqrt{p^2 + (rq)^2} \tag{35}$$

from which we derive $\dot{\mathbf{e}} \sim \partial G_c/\partial \boldsymbol{\sigma}$. For a lack of knowledge we chose $r = 1$ and assume for the moment orthotropic creep deformations. If creep due to shear would become important for applications one must perform, in addition to the uniaxial creep tests, some tests for shear creep to determine the other components of the strain tensor or triaxial creep experiments to determine r. The creep model is general enough to account for these properties if necessary.

During uniaxial compression we have $\sigma_{yy} > \sigma_{xx} = \sigma_{zz}$. We can evaluate from equation (33) e.g. the strain rate component $\dot{e}_{xx}$ and find

$$\dot{e}_{xx} \sim 20\sigma_{xx} - 7\sigma_{yy} - 7\sigma_{zz} \tag{36}$$

which is equivalent to

$$\dot{e}_{xx} \sim 9\sigma_{xx} + 7p. \tag{37}$$

The same results hold for the other components. Normalization such that $\dot{e}_{xx}+\dot{e}_{yy}+\dot{e}_{zz} = \dot{\varepsilon}_c$ finally yields

$$\dot{e}_{xx} = \frac{\dot{\varepsilon}_c}{6}\left(9\frac{\sigma_{xx}}{p} + 7\right), \tag{38}$$

$$\dot{e}_{yy} = \frac{\dot{\varepsilon}_c}{6}\left(9\frac{\sigma_{yy}}{p} + 7\right), \tag{39}$$

$$\dot{e}_{zz} = \frac{\dot{\varepsilon}_c}{6}\left(9\frac{\sigma_{zz}}{p} + 7\right). \tag{40}$$

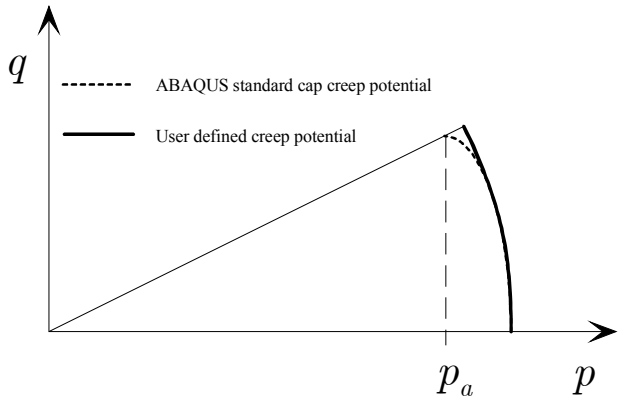

Figure 17: Cap creep potentials

These strain rates can not be used directly for a code input in the ABAQUS creep laws. However, the user subroutine UEXPAN foreseen for modelling of user defined incremental strain allows to define Δe_{xx}, Δe_{yy}, and Δe_{zz}. This is done by integration of equations (38)-(40) over the time increment Δt.

For the time integration we assume for simplicity that the stress and temperature stay constant for the time interval Δt considered. This causes no serious restriction since the time step during calculations can be chosen small enough that the final results are nearly unaffected by this simplification. On the other hand, the temperature is kept constant during the whole experiment and the stress varies only during the initial loading time which is negligible compared with the total time of the experiment. Nevertheless, the loading cycle is resolved in the present calculations by a high number of time increments so that the results are accurate even for varying stress. We use the constitutive equation (25) to define the creep strain rate and integrate forward in time with A and p kept constant during the time step. This yields

$$\Delta\varepsilon_c = \frac{1}{m+1} A p^n t_0^{m+1} \left[\left(1 + \frac{\Delta t}{t_0} \right)^{m+1} - 1 \right] \tag{41}$$

or with the magnitude of creep strain ε_{c0} at the beginning of the time step

$$\Delta\varepsilon_c = \varepsilon_{c0} \left[\left(1 + \frac{\Delta t}{t_0} \right)^{m+1} - 1 \right]. \tag{42}$$

The variable t_0 is a fictive time which is determined from the accumulated creep deformation, the current load and thermal conditions, i.e.

$$t_0 = \hat{t} \left[\frac{\varepsilon_{c0}}{\hat{\varepsilon}_c} \frac{\hat{A}}{A} \left(\frac{\hat{p}}{p} \right)^n \right]^{\frac{1}{m+1}}, \tag{43}$$

where the quantities $\hat{\varepsilon}_c$, $\hat{t}$, $\hat{A}$, $\hat{p}$ are taken from a reference experiment.

In a next step we complete the creep model by introducing the appropriate temperature dependence. The temperature dependence for thermally activated creep of ceramic materials may be described according to Munz and Fett (1999) by

$$A = C \exp\left(-\frac{Q}{RT}\right), \tag{44}$$

where Q is the activation energy and R is the gas constant. Such a behavior is observed also for beds of granular breeder materials and described by Reimann and Wörner (2000). In equation (43) only the ratio $\hat{A}/A$ is important. Therefore we do not need to determine the value of C and we find directly

$$\frac{\hat{A}}{A} = \frac{\exp\left(-\frac{Q}{R\hat{T}}\right)}{\exp\left(-\frac{Q}{RT}\right)}. \tag{45}$$

The quantity Q/R has been determined by Reimann and Wörner (2000) from a number of experiments and given as $Q/R = 10.22 \cdot 10^3\,\mathrm{K}$.

The model has been calibrated with the creep experiment performed by Reimann and Wörner (2000) at 800 °C. The best agreement between the numerical predictions and the experimental data is achieved if we chose the exponent for time and pressure dependence as $m = -0.82$ and $n = 0.705$. These values are close to those given by Reimann and Wörner (2000) who propose values as $m = -0.8$ and $n = 0.65$ for a fit of a number of experiments. The magnitude of creep strain and the reference time are $\hat{\varepsilon}_c = 3.12 \cdot 10^{-2}$ and $\hat{t} = 5000\,\mathrm{min}$ and $\hat{p} = 2.62\,\mathrm{MPa}$.

During the loading phase the granular bed undergoes some initial compression caused by inelastic granular deformation and creep as shown in Fig. 18. During this period the vertical load is increased linearly up to its final value. The fraction of creep deformation during the loading period is already comparable with (for 800 °C) or even larger (for 900 °C) than the permanent plastic deformation without creep, given by the curve for low temperature. At temperatures lower than 400 °C thermal creep is irrelevant. The long term behavior can be seen more clearly from Fig. 19. The reference case with $T = 800\,^\circ\mathrm{C}$ is reproduced well. There is almost no difference between the numerical predictions and the experiment. Thermal creep for $T < 400\,^\circ\mathrm{C}$ is negligibly small. The sample is deformed during the loading phase and nearly keeps this deformation for the whole time of the experiment.

Thermal creep leads to monotonic increase of contact surfaces between the particles. This changes both, the elastic properties of the material and the granular behavior during compaction with the result that the cap position is modified. As a consequence the bed would behave stiffer during a second increase of the load. This effect has been observed during experiments and it will be taken into account for calculations in which a second increase of the load occurs. We disregard for the moment the change in the elastic properties and focus our attention on the cap hardening due to thermally activated creep, say on creep hardening. It is straightforward to incorporate creep hardening depending on the accumulated creep strain ε_c in the cap hardening equation (24) as

$$p_b = \hat{p}_b \left(\frac{\varepsilon_{vol,pl} + \varepsilon_c}{\hat{\varepsilon}_{vol,pl}}\right)^a, \tag{46}$$

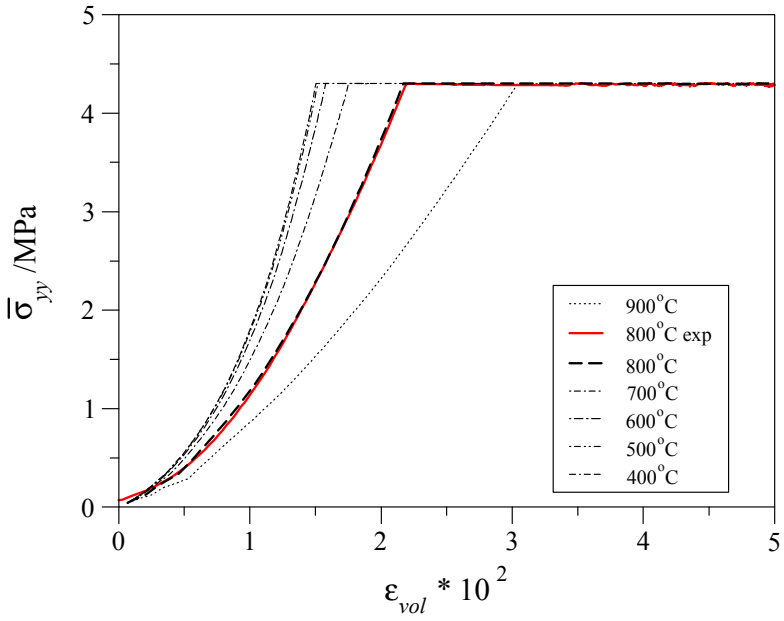

Figure 18: Vertical load versus volumetric strain for various temperatures. The case of 800 °C is compared to experimental results.

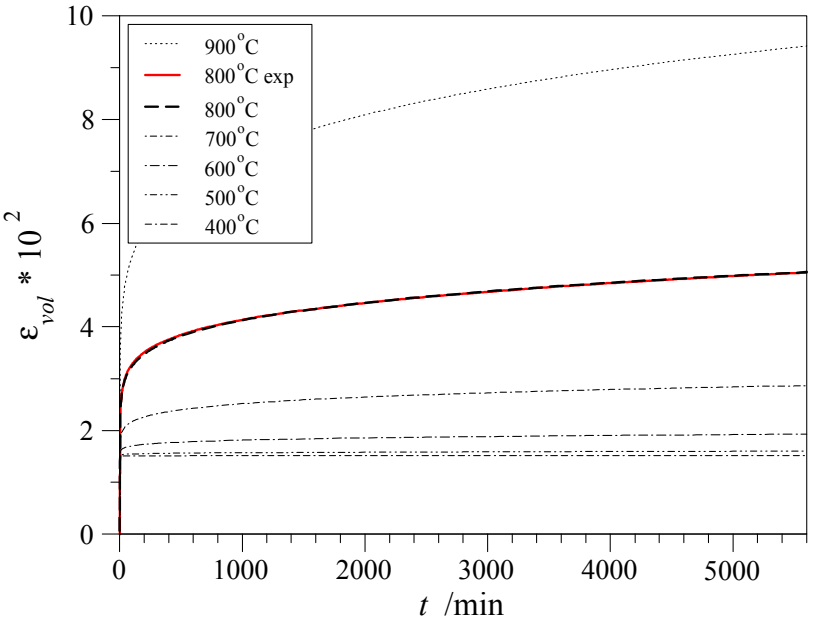

Figure 19: Volumetric strain versus time for various temperatures. The load is increased linearly up to $\bar{\sigma}_{yy} = 4.3$ and kept constant at this value for $t > 5$ min. The case of 800 °C is compared to experimental results.

and we apply this equation for most of the creep phase, except for the very short transients in which the load is increased. The reason is very simple. Suppose there would be a compression without creep, then we would have a result similar to that at low temperature as shown in Fig. 18. The applied vertical load $\bar{\sigma}_{yy}$ is related to the total volumetric strain ε_{vol} as shown by the line for 400 °C and creep is irrelevant. If creep is active during the time when the load is increased the sample exhibits larger deformations which are caused by consolidation as for low temperatures plus deformations due to creep. The granular bed behaves softer for a compression for which creep is active. However, if we would apply equation (46) during this phase the result would be that the sample behaved stiffer compared with a case where creep is not active since p_b increases with creep strain. To resolve this contradiction we replace ε_c in equation (46) by ε_c' and determine this quantity as

$$\varepsilon_c' = \int_{t_0}^{t} \dot{\varepsilon}_c \, dt \tag{47}$$

for the times $t > t_0$. Here, t_0 is the time at which the load has reached the final magnitude. In the experiment the time during which the load is applied is very small compared with the total time during which creep is active, $t_0/t_{\max} < 10^{-3}$, so that this assumption seems to be justified. We keep all other parameters as they were introduced above. We repeat the calculations for the same cases as shown previously with $\bar{\sigma}_{yy} = 4.3\,\mathrm{MPa}$ for $t_0 = 5\,\mathrm{min} < t < 5600\,\mathrm{min}$. We increase the load in a second step linearly to $\bar{\sigma}_{yy} = 8.58\,\mathrm{MPa}$ and keep it constant for $5605\,\mathrm{min} < t < 12850\,\mathrm{min}$. The results are shown in Figs. 20 and 21. The first part of the figures has been already shown during the discussion of creep at constant load. A comparison with the experimental data at 800 °C shows here a perfect agreement also for the second step after the external load is raised.

We observe from calculations strain magnitudes of $\varepsilon_{vol} > 0.08$. For higher temperatures the model would predict even larger creep strain rates. If the creep model predicts, e.g. for higher temperatures, volumetric deformations which become of the same order of magnitude as the void fraction of the granular bed, it is obvious that the creep mechanism must change since an extrapolation to larger times could predict a density of the bed which is higher than the density of the particles.

We have seen already from Fig. 18 that for high temperatures creep gives an essential contribution to the strain magnitude already during the initial period when the load is applied. This fact is analyzed in the following by using for the stress increase different load ramps between 0.15 MPa / min and 4.7 MPa / min as shown in Fig. 22. The load ramps used for the calculations and the temperatures correspond to values used in experiments (Bühler and Reimann (2001)). Note, during experiments one observes typically a very small (negligible) stress increase with initial volumetric strain ε_0. The values of ε_0 depend rather on the initial conditions than on the applied load. This behavior may be explained by a rearrangement of particles near the walls or in the bed. The experimental results plotted in Fig. 22 show the vertical load $\bar{\sigma}_{yy}\,(\varepsilon_{vol} - \varepsilon_0)$ where we used $\varepsilon_0 = 0.003$, 0.003, 0.0002, and 0.001, for the cases with 0.15, 2.8, 4.7 MPa / min, and for no-creep, respectively. We observe large creep strain during the loading period if the load ramp is very small, i.e. when the material finds enough time to deform. For fast ramps (shorter time) the deformation due to creep is smaller. For a comparison

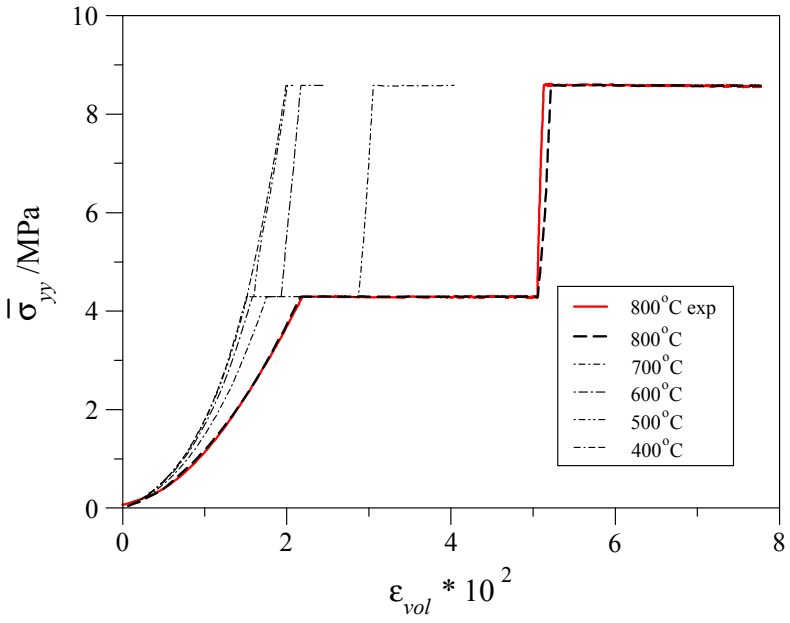

Figure 20: Vertical load versus volumetric strain for various temperatures. The case of 800 °C is compared to experimental results.

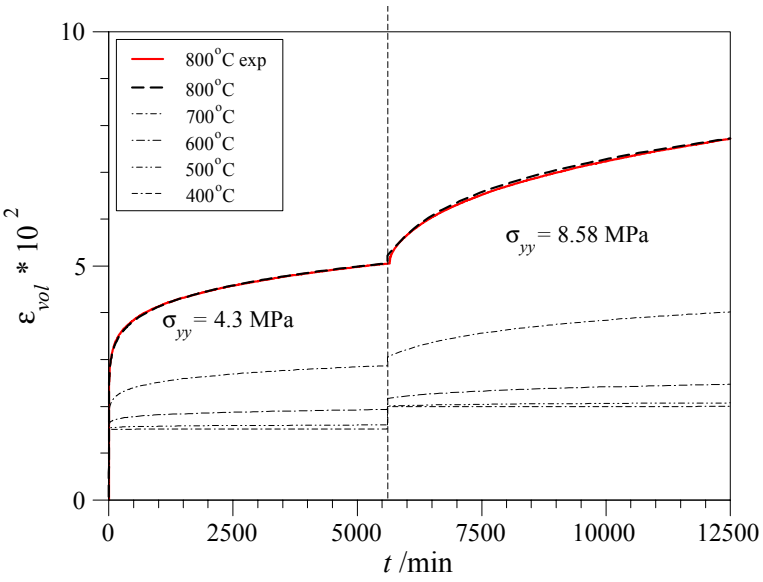

Figure 21: Volumetric strain versus time for various temperatures. The load is increased linearly up to $\bar{\sigma}_{yy} = 4.3\,\mathrm{MPa}$ and kept constant at this value for $t > 5\,\mathrm{min}$. A second increase of the load takes place after 5600min. For $t > 5605\,\mathrm{min}$ the new load stays at $\bar{\sigma}_{yy} = 8.58\,\mathrm{MPa}$. The case of 800 °C is compared to experimental results.

and as a check of the numerical procedure two loading cycles at low temperature are added to the diagram. In fact, for low temperature, creep during the loading period is negligible and results become therefore independent of the load ramps.

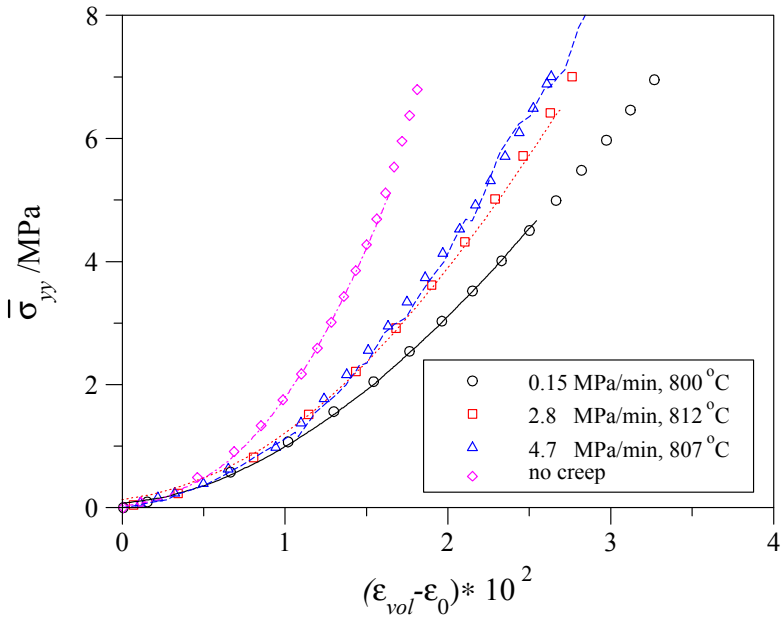

Figure 22: Influence of different load ramps on thermally activated creep.

The creep behavior as a function of time is shown in Fig. 23 for the two investigated load ramps of 0.17 MPa / min and 2.8 MPa / min. After the vertical stress reaches a level of 6.5 MPa this magnitude is held constant for the rest of the creep experiment. It can be seen from the figure that the creep strain rates differ during the loading period and even some time later. However, on a longer time scale the remaining difference becomes insignificant.

In applications for fusion blankets the load is established by differences in thermal expansion coefficients between the granular material and the confining walls. Under such constraints thermal creep will relax stresses during the operation of the blanket. In order to investigate such effects the third type of experiments has been performed in which the granular bed has been compressed up to $\sigma_{yy} = 8\,\mathrm{MPa}$ to simulate the thermally induced loads (Bühler and Reimann (2001)). Then the vertical load has been manually controlled in order to keep the piston in a constant position while the vertical force (vertical stress) is recorded (see Fig. 24). This manual control was crucial in a sense that vertical load amplitudes up to 1 MPa were required in order to reestablish the initial position of the plate. The agreement between theory and experiment in the initial stage is not satisfactory. However, for 770 °C the experimental data approach the theoretical one for the long-term behavior. It can be seen that after a time less than one hour the stress is released to a fraction of the initial value. This means that at higher temperatures thermal stresses do not cause severe problems if the thermal ramps are slow enough that stresses can be released by thermal creep. For high temperatures a decrease of stress according to a power law $\sigma_{yy} \sim t^{-0.2}$ is observed.

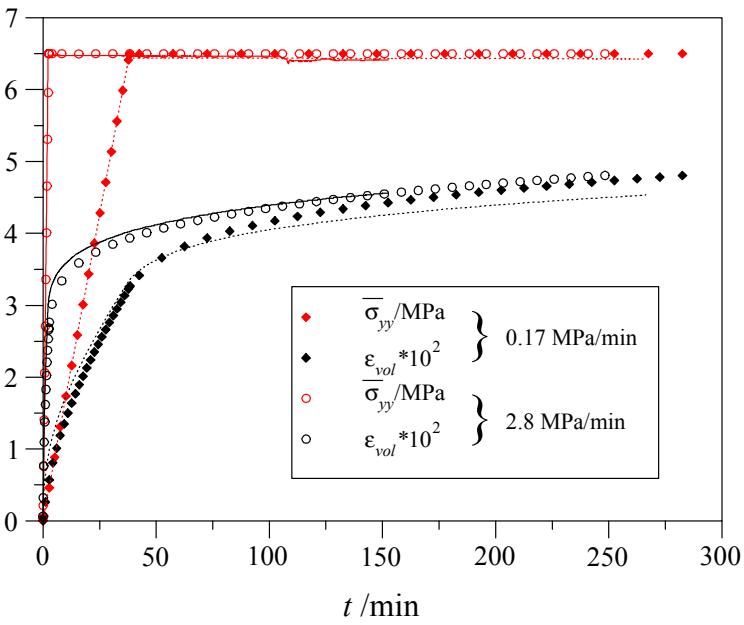

Figure 23: Influence of different load ramps on long-term thermally activated creep.

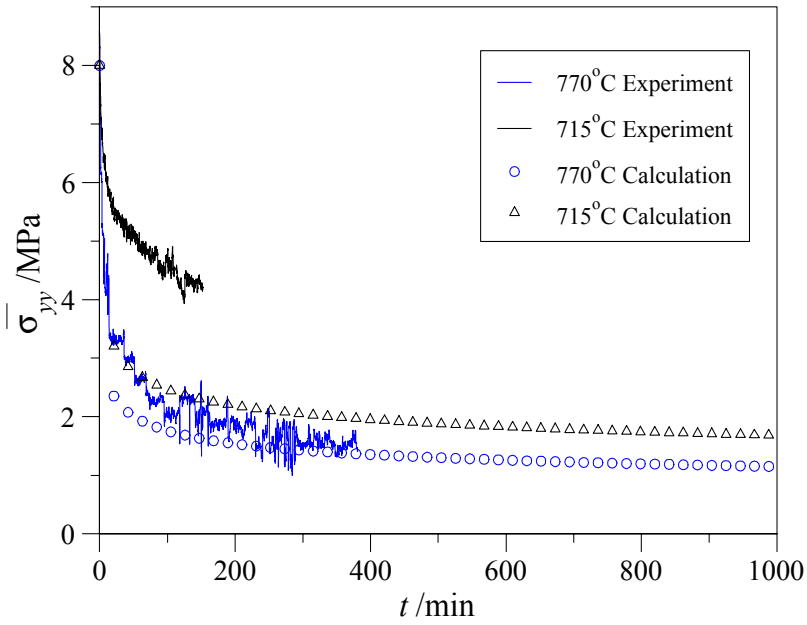

Figure 24: Stress release by thermal creep. Vertical component of stress as a function of time

5 Conclusions

Continuum models are efficient means for the determination of the mechanical behavior of granular breeder materials in fusion blankets. Such models account for various effects such as nonlinear elasticity, granular flow of particles due to shear failure or consolidation, and thermally activated creep.

The mechanical behavior of Li_4SiO_4 pebble beds at ambient temperature was investigated using a blanket typical geometry where the bed is mechanically compressed in the vertical (poloidal) direction, simulating the stresses caused by thermal expansion of the breeder material. The bed is allowed to expand horizontally, simulating granular particle flow due to radial stress profiles caused in the blanket by radial temperature gradients.

It is shown that for densely filled beds the horizontal movements become negligible for already quite small lateral loads. From this observation one might conclude that for blanket conditions the flow of particles is not very expressed. There are two consequences:

- Compared to a stress release if particles would move, higher local internal stresses occur which result in a larger thermomechanical interaction between pebble beds and structural material;
- The computational description of this interaction becomes simpler as well as the experimental effort to generate the required input data for numerical codes: internal friction and wall friction are less important and the required data could be obtained essentially by uniaxial compression tests.

The strong influence of the initial state of the pebble beds on the mechanical behavior has been shown. It must be ensured that experiments used to calibrate computational tools use the same methods as in the blanket to get a dense packing (e.g. vibrations). These computational models used to predict the behavior of pebble beds assume quasi steady state conditions. In blankets a quite fast load increase during start-up is expected which will change the bed behavior. This effect, should be quantified in future experiments.

Thermal creep of solid breeder materials has been investigated. Experiments performed at elevated temperatures close to the operating temperatures in fusion blankets show that the creep strain reaches values as large as the elastic and plastic granular deformations. The time after which these large creep deformations occur is relatively small (some hours). This has the consequence that thermally induced loads in the pebble beds or loads due to irradiation swelling are continuously released by creep of the breeder material and should not cause severe problems at high temperatures. Continuum models are efficient means for the determination of the mechanical behavior of granular breeder materials in fusion blankets. Such models account for various effects such as nonlinear elasticity, granular flow of particles due to shear or consolidation, and thermally activated creep. The modelling of thermally activated creep is possible by using a modified cap-creep potential. The new creep potential has been implemented in a user defined subroutine and yields results which agree well with experimental data.

References

ABAQUS / Standard: 1996, Hibbitt, Karlsson & Sorensen, INC.

Boccaccini, L.: 2000, Advanced helium cooled pebble bed blanket, *Technical Report FZKA 6402*, Forschungszentrum Karlsruhe.

Bühler, L. and Reimann, J.: 2001, Thermal creep of granular breeder materials in fusion blankets, *10th International Conference on Fusion Reactor Materials, October 14-19, 2001, Baden Baden.*

Bühler, L., Reimann, J., Arbogast, E. and Thomauske, K.: 2000, Mechanical behavior of Li4SiO4 pebble beds in a blanket typical geometry, *Fusion Engineering and Design* **49-50**, 499–505.

Dalle Donne, M., Fischer, U., Norajitra, P., Reimann, G. and Reiser, H.: 1995, European DEMO BOT solid breeder blanket: The concept based on the use of cooling plates and beds of beryllium and Li_4SiO_4 pebbles, *in* K. Herschbach, W. Maurer and J. E. Vetter (eds), *Fusion Technology 1994*, Vol. 2, Elsevier, pp. 1157–1160.

Durelli, A. J., Phillips, E. A. and Tsao, C. H.: 1958, *Introduction to the Theoretical and Experimental Analysis of Stress and Strain*, McGraw-Hill Series in Mechanical Engineering, McGraw-Hill Book Company, INC.

Endres, A. L.: 1990, The effect of contact generation on the elastic properties of a granular medium, *Transactions of the ASME* **57**, 330–336.

Hermsmeyer, S., Gordeev, S., Kleefeldt, K., Schleisiek, K., Schmuck, I., Schnauder, H., Fischer, U., Malang, S., Fütterer, M. and Ogorodnikowa, O.: 1999, Improved helium cooled pebble bed blanket, *Technical Report FZKA 6399*, Forschungszentrum Karlsruhe.

Hunter, S. C.: 1983, *Mechanics of continuous media*, Ellis Horwood Series in Mathematics and its Applications, 2nd edn, Ellis Horwood Limited.

Munz, D. and Fett, T.: 1999, *Ceramics Mechanical Properties, Failure Behaviour, Materials Selection*, Springer Series in Materials Science, Springer-Verlag, Berlin/Heidelberg.

Nedderman, R. M.: 1992, *Statics and kinematics of granular materials*, Cambridge University Press.

Reimann, J. and Müller, S.: 1998, First experiments on the thermomechanical behaviour of Li_4SiO_4 pebble beds., *Fusion Technology 1998, Proceedings of the 20th Symposium on Fusion Technology, Marseille, September 7-11, 1998*, Vol. 2, pp. 1337–1340.

Reimann, J., Müller, S., Arbogast, E. and Thomauske, K.: 1998, Experiments on the thermomechanical behaviour of ceramic pebble beds, *Technical Report FZKA 6148*, Forschungszentrum Karlsruhe.

Reimann, J. and Wörner, G.: 2000, Thermal creep of Li4SiO4 pebble beds, *Fusion Technology 2000, 21th Symposium on Fusion Technology, Madrid, September, 11-15, 2000*.

Walton, K.: 1987, The effective elastic moduli of a random packing of spheres, *J. Mech. Phys. Solids* **35**(2), 213–226.